



Universidad Autónoma
de Madrid

Biblos-e Archivo
Repositorio Institucional UAM

Repositorio Institucional de la Universidad Autónoma de Madrid

<https://repositorio.uam.es>

Esta es la **versión de autor** del artículo publicado en:
This is an **author produced version** of a paper published in:

CrystEngComm 20.34 (2018): 5033-5044

DOI: <https://doi.org/10.1039/c8ce00919h>

Copyright: © The Royal Society of Chemistry 2018

El acceso a la versión del editor puede requerir la suscripción del recurso
Access to the published version may require subscription

On the importance of Pb \cdots X (X = O, N, S, Br) tetrel bonding interactions in a series of tetra- and hexa-coordinated Pb(II) compounds†

Saikat Kumar Seth,^a Antonio Bauzá,^{ab} Ghodrat Mahmoudi,^b Vladimir Stilinović,^d Elena López-Torres,^e Guillermo Zaragoza,^f Anastasios D. Keramidas^g and Antonio Frontera^{*b}

Five new Pb(II) complexes of hydrazone-based and Schiff-based ligands and three different anionic co-ligands (azide, thiocyanate and bromide) have been synthesized and characterized by structural, analytical and spectroscopic methods. This variety of ligands can coordinate to the Pb(II) metal center in a tridentate or tetradentate fashion via a different combination of any of nitrogen, oxygen and sulphur donor atoms. Moreover, the organic ligands can be in mono-deprotonated or neutral forms. By using single-crystal X-ray crystallography, we show that the synthesized complexes aggregate into larger supramolecular entities due to the formation of noncovalent tetrel bonding interactions. The Pb(II) center is hemidirectionally coordinated even in those complexes where the coordination number is six. Consequently, this is sterically ideal for establishing tetrel bonding interactions with electron-rich nitrogen, bromide or sulphur atoms. These contacts are significantly larger than the sums of the covalent radii. Hence, they can be described as non-covalent tetrel bonding interactions. They interconnect the covalently bonded units into supramolecular assemblies (dimers or tetramers). The contribution of contacts involving the Pb atom has been studied using Hirshfeld surface analysis and fingerprint plots. We have analysed the supramolecular assemblies observed in the solid state by means of DFT calculations and characterized them using Bader's theory of atoms-in-molecules.

Introduction

Lead is a deadly toxic element regarded as a biological poison similar to mercury.¹ Lead presents a highly versatile coordination chemistry because of its large radius and ability to adopt different coordination numbers. Therefore, it has attracted

synthetic inorganic chemists to prepare a variety of new lead(II) complexes.² Despite its bad reputation (negative roles related to pollution and health), lead-containing materials are utilized in the fabrication of batteries, ferroelectric and non-linear optical materials, and semiconductors.³ Further interest in the study of lead coordination compounds comes from the necessity to develop new ligands to trap lead(II), either from the human body for the treatment of lead intoxication or for the removal of lead from drinking water or paints.^{4,5} A convenient approach to prepare lead(II) complexes is to use N₂O₂/N₄ donor compartmental Schiff bases. These complexes have applications in several areas like gas separation and encapsulation and transport and activation of small molecules⁶ among others.^{7–9} The 6s² electron pair of Pb(II) remains as an inert pair mainly.¹⁰ The extent to which the lone pair is stereochemically active¹¹ has been studied and discussed before in the literature.¹²

In addition to the widely used hydrogen bonding interactions for the construction of supramolecular metal organic frameworks (SMOFs), other directional interactions such as σ -hole tetrel bonding interactions are becoming interesting players.¹³ Indeed, strong σ -hole interactions occur in complexes where a heavy atom of group IV (tin and lead) is

^a Department of Physics, Jadavpur University, Kolkata 700032, India

^b Departament de Química, Universitat de les Illes Balears, Crta. de Valldemossa km 7.5, 07122 Palma, Balears, Spain. E-mail: toni.frontera@uib.es

^c Department of Chemistry, Faculty of Science, University of Maragheh, P.O. Box 55181-83111, Maragheh, Iran. E-mail: mahmoudi_ghodrat@yahoo.co.uk

^d Department of Chemistry, Faculty of Science, University of Zagreb, Horvatovac 102a, HR-10000 Zagreb, Croatia

^e Departamento de Química Inorgánica, Facultad de Ciencias, Módulo 07, Universidad Autónoma de Madrid, Crta. de Colmenar Viejo, Km 15, 28049 Madrid, Spain

^f Unidad de RX, Edificio CACTUS, Campus Vida, Santiago Compostela, 15782, Spain

^g Department of Chemistry, University of Cyprus, 1678 Nicosia, Cyprus

† Electronic supplementary information (ESI) available. CCDC 1840504–1840508 contain the supplementary crystallographic data for compounds 1–5; Tables S1–S4 list the bond lengths and angles and geometric parameters of noncovalent interactions. Fig. S1–S5 represent the supramolecular assemblies; Fig. S6 and S7 represent Hirshfeld surfaces and fingerprint plots. For ESI and crystallographic data in CIF or other electronic format see DOI: 10.1039/c8ce00919h

covalently bonded to electronegative ones.¹⁴ For instance, the construction of lead(II) SMOFs based on covalent and non-covalent tetrel bonding has been reported.^{15–17} In these SMOFs, Pb \cdots N/S tetrel bonding interactions interconnect the covalently bonded units into supramolecular assemblies. In fact, tetrel bonds with hemi-directionally coordinated lead commonly occur with high predictable geometries, thus playing an important role in the solid-state chemistry of lead. As a matter of fact, the divalent form of lead (Pb²⁺) presents a special interest for physical chemists due to its coordination and organization properties, namely, holodirected and hemidirected (Fig. 1).¹⁸ Lead(II) with a variety of N/O/X donor ligands (X = halide or pseudohalide) is hemidirected for coordination numbers of up to five ($n \leq 5$), and holodirected for coordination numbers of six and higher ($n \geq 6$).¹⁹

In the present work, we used five different Schiff base ligands, HL¹ [3-pyridinecarboxylic acid, 2-(phenyl-2-pyridinylmethylene)hydrazide], HL² [4-pyridinecarboxylic acid, 2-(phenyl-2-pyridinylmethylene)hydrazide], H₂L³ {2-pyridinecarboxylic acid, 2,2'-(1,2-diphenyl-1,2-ethanediylidene)-dihydrazide}, L⁴ {1,2-ethanedione, 1,2-diphenyl-1,2-bis[2-[1-(2-pyridinyl)ethylidene]hydrazone]} and HL⁵ {hydrazinecarbothioamide, 2-[1-(2-pyridinyl)ethylidene]} (see Scheme 1). This variety of ligands provides many different possibilities of coordination in both the number and types of donor atoms (N, O and S). In this manuscript, we analyse their complexes with Pb(II) and, in particular, their ability to form either holodirected or hemidirected coordination compounds. Interestingly, some of the complexes present a coordination number (n) of 6 and, unexpectedly, the type of coordination is hemidirectional instead of holodirectional.

The solid state structures of complexes 1–5 (see Scheme 2) have been determined by single crystal X-ray diffraction analyses. Interestingly, in all complexes the lead(II) atom participates in non-covalent tetrel bonding interactions. These forces along with other non-covalent interactions are crucial to understand the supramolecular assemblies and organometallic frameworks observed in their solid state architecture. The lead(II) ion presents a coordination mode (hemidirectional) in which it has a clear void in the distribution of bonds to the ligands. Remarkably, this is observed

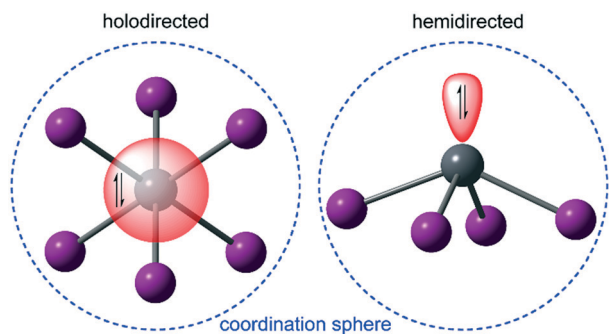
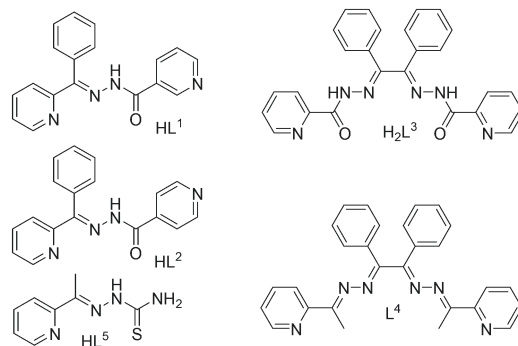


Fig. 1 Graphic representation of the holodirected (left) and hemidirected (right) coordination modes of lead(II). The location of the inert LP is also indicated.



Scheme 1 Ligands used in this work.

even in those with $n = 6$. This fact facilitates the approach of electron donors enabling the formation of a strong tetrel bond with a predictable geometry. We have used DFT calculations to study the nature and strength of the tetrel bonds in the structures, which evidenced the existence of a σ -hole at the lead atom.

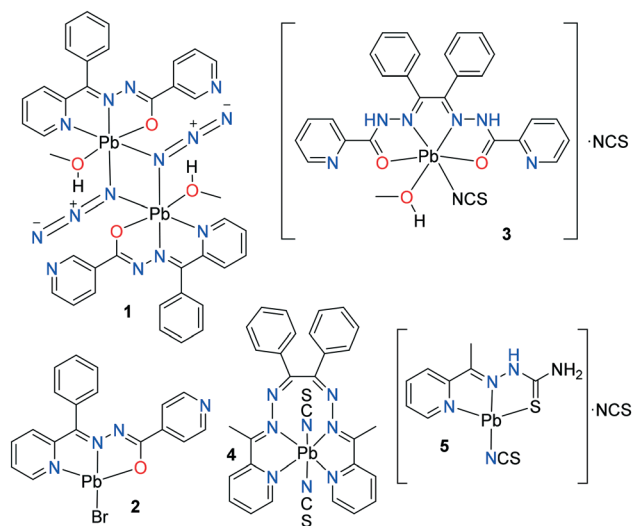
Experimental and theoretical methods

Synthesis of the ligands

All reagents and solvents are commercially available and were used without further purification. The ligands (see Scheme 1) were prepared in the laboratory following a literature method.²⁰ All other materials are commercially available and reagent grade and were used as purchased without further purification.

Synthesis of complexes 1–5

Due to the insolubility of these compounds in most of the common solvents employed, we failed to crystallize the materials as single crystals, but rather as polycrystalline powders. We found a solution to our inability to grow single crystals, which is the use of very interesting and unusual glassware



Scheme 2 Complexes 1–5 reported in this work.

for reaction/crystallization apparatus (a branched tube) recently developed by us.²⁰ The detailed synthesis of **1** is described here. The rest of the complexes were synthesized using the same procedure, mixing equimolar quantities of the appropriate PbX₂ salts (X = CH₃COO, Br, SCN) with HL¹, HL², H₂L³, L⁴ and HL⁵, respectively.

Synthesis of 1: Pb(CH₃COO)₂ (0.164 g, 0.5 mmol), NaN₃ (0.065 g, 1 mmol) and HL¹ (0.113 g, 0.5 mmol) were placed in the main arm of a branched tube. Methanol (15 ml) was carefully added to fill the arms. The tube was sealed and immersed in an oil bath at 60 °C while the branched arm was kept at ambient temperature. After 5 days, crystals of **1** that were isolated in the cooler arm were filtered off, washed with acetone and ether, and dried in air.

Pb₂(MeOH)₂(L¹)₂(μ_{1,1}-N₃)₂ (1**).** The isolated yield was 87%. Anal. calcd. (found) for C₃₈H₃₄N₁₄O₄Pb₂; C, 39.17 (36.91); H, 2.94 (2.75); N, 16.83 (16.95) %. IR (cm⁻¹) selected bands: $\tilde{\nu}$ = CH b (oop): 668 (m) and 698 (m); CCst: 1464 (m); C=N st: 1511 and 1546 (m); C–O st (ligand) 1585; N₃ st: 2031 (w); OH st: 3430 (w) cm⁻¹.

[Pb(L²)(Br)]·H₂O (2**).** The isolated yield was 89%. Anal. calcd. (found) for C₁₈H₁₆BrN₄O₂Pb; C, 35.59 (35.32); H, 2.66 (2.73); N, 9.22 (9.38) %. IR (cm⁻¹) selected bands: $\tilde{\nu}$ = CH b (oop): 711 (m) and 753 (m); CCst: 1411 (m); C=N st: 1521 and 1583 (m); C–O st (ligand) 1646; CH st: 2891 (w), OH st: 3480 (w) cm⁻¹.

[Pb(MeOH)₂(H₂L³)(NCS)][NCS] (3**).** The isolated yield was 85%. Anal. calcd. (found) for C₂₉H₂₄N₈O₃PbS₂; C, 43.33 (43.51); H, 3.01 (2.88); N, 13.94 (14.02) %. IR (cm⁻¹) selected bands: $\tilde{\nu}$ = CH b (oop): 617 (m) and 750 (m); CCst: 1488 (m); C=N st: 1613 (s); C=O st (ligand) 1663; SCN: 2013 and 2066; CH st: 2926 and 3057 (w); NH: 3288 (m); OH st: 3430 (w) cm⁻¹.

Pb(L⁴)(NCS)₂ (4**).** The isolated yield was 85%. Anal. calcd. (found) for C₆₂H₅₆N₁₆O₂Pb₂S₄; C, 46.55 (46.46); H, 3.53 (3.28); N, 14.01 (14.22) %. IR (cm⁻¹) selected bands: $\tilde{\nu}$ = CH b (oop): 693 (m) and 741 (m); CCst: 1470 (m); C=N st: 1579; SCN: 2060; CH st: 2922 and 3059 (w); OH st: 3452 (w) cm⁻¹.

Pb(L⁵)(NCS)₂ (5**).** The isolated yield was 85%. Anal. calcd. (found) for C₁₀H₁₀N₆PbS₃; C, 23.20 (23.11); H, 1.95 (1.88); N, 16.24 (16.32) %. IR (cm⁻¹) selected bands: $\tilde{\nu}$ = CH b (oop): 608 (m) and 770 (m); CCst: 1467 (m); C=N st: 1525 and 1580 (m); C=S st (ligand) 1542; SCN: 2032 and 2062; CH st: 2926 (w); NH: 3210 (m) and 3313 (m) cm⁻¹.

Physical measurements

For the physical measurements, FTIR spectra were recorded on a Bruker Tensor 27 FTIR spectrometer. Microanalyses were performed using an Elementar vario EL III analyser.

X-ray crystallography

Single crystals of **1**–**5** suitable for X-ray analysis were selected and mounted on a glass fiber, and crystallographic data were collected using an Oxford Diffraction Xcalibur Onyx (1), a Rigaku Mercury 1K (2), a Bruker APEX-II CCD (3 and 5), and

an Oxford Diffraction Xcalibur CCD (4) diffractometer using MoK α radiation (λ = 0.71073 Å) in the ω - or ω - and ϕ -scan mode. The data were collected using Mo K α (2, 3, 4, 5) or Cu K α (1) radiation at room temperature (1, 3, 4), 183 K (2) or 100 K (5).

The detector frames were integrated by the use of the programs CrysAlis RED,²¹ CrysAlisPro,²² CrystalClear²³ and SAINT²⁴ and the empirical absorption corrections were performed using the SCALE3 ABSPACK,²¹ and SADABS²⁵ programs. All the structures were solved by direct methods and refined by full matrix least-squares procedures in SHELXTL.²⁶ Hydrogen atoms were placed on calculated positions using a riding model as the proximity of lead atoms made it impossible to locate their positions from electron difference maps. In the structures comprising coordinated methanol molecules (**1** and **3**), the orientation of the hydroxyl group was determined from the molecular geometry and the hydrogen atom refined as riding on the parent oxygen. The structure of **4** contained a non-coordinated methanol solvent molecule in severe disorder so no reasonable assignment of the hydrogen atoms on the solvent molecule was possible. The crystallographic data and refinement details are given in Table 1.

Hirshfeld surface analysis

The molecular Hirshfeld surfaces^{27,28} of the title crystal structures were constructed based on the electron distribution calculated as the sum of spherical atom electron densities.²⁰ The normalized contact distance (d_{norm}) based on both d_e and d_i and the vdW radii of the atom, given by eqn (1), enables the identification of the regions of particular importance to intermolecular interactions.²⁷ The combination of d_e and d_i in the form of a 2D fingerprint plot²⁹ provides a summary of the intermolecular interactions in the crystal.²⁷ The Hirshfeld surfaces were mapped with d_{norm} , and the 2D fingerprint plots presented here were generated using *CrystalExplorer 3.1*.³⁰

$$d_{\text{norm}} = \frac{d_i - r_i^{\text{vdw}}}{r_i^{\text{vdw}}} + \frac{d_e - r_e^{\text{vdw}}}{r_e^{\text{vdw}}} \quad (1)$$

Theoretical methods

The geometries of the complexes reported in this work were computed at the M06-2X/def2-TZVP level of theory using the crystallographic coordinates within the TURBOMOLE program.³¹ The M06-2X functional is adequate because it provides a correct description of the intermediate-range van der Waals interactions, due to the inclusion of the kinetic energy density, which helps to identify weak non-covalent bonds as reported herein. The basis set superposition error for the calculation of interaction energies has been corrected using the counterpoise method.³² The “atoms-in-molecules” (AIM)³³ analysis of the electron density has been performed at the same level of theory using the AIMAll program.³⁴

Table 1 Crystal data and structure refinement parameters for 1–5

Structure	1	2	3	4	5
Empirical formula	C ₃₈ H ₃₄ N ₁₄ O ₄ Pb ₂	C ₁₈ H ₁₅ Br ₁ N ₄ O ₂ Pb ₁	C ₂₉ H ₂₄ N ₈ O ₃ Pb ₁ S ₂	C ₆₂ H ₅₆ N ₁₆ O ₂ Pb ₂ S ₄	C ₁₀ H ₁₀ N ₆ Pb ₁ S ₃
Formula weight	1165.17	606.44	803.87	1599.84	517.61
Temperature (K)	293(2)	183(2)	296(2)	293(2)	100(2)
Wavelength (Å)	1.5418	0.71073	0.71073	0.71073	0.71073
Crystal system	Monoclinic	Triclinic	Triclinic	Triclinic	Monoclinic
Space group	<i>P</i> 2 ₁ / <i>c</i>	<i>P</i> $\bar{1}$	<i>P</i> $\bar{1}$	<i>P</i> $\bar{1}$	<i>P</i> <i>c</i>
<i>a</i> , <i>b</i> , <i>c</i> (Å)	10.9860(4), 21.7326(7), 8.8856(4)	9.2807(13), 10.2962(15), 10.9703(13)	10.3837(2), 11.5738(3), 14.3370(3)	9.7763(6), 11.3341(7), 15.0580(10)	9.0368(7), 11.3777(10), 7.6503(6)
α , β , γ (°)	90, 108.941(4), 90	103.736(2), 105.229(3), 102.200(2)	95.2160(10), 90.1200(10), 113.7360(10)	105.607(7), 91.747(6), 101.222(6)	90.00, 112.279(4), 90.00
Volume (Å ³)	2006.60(14)	939.7(2)	1569.31(6)	1570.19(18)	727.87(10)
<i>Z</i> /density (calc.) (Mg m ⁻³)	2/1.928	2/2.143	2/1.699	1/1.692	2/2.362
Absorption coefficient (mm ⁻¹)	16.613	11.122	5.552	5.544	12.017
<i>F</i> (000)	1112	568	782	784	484
Crystal size (mm ³)	0.35 × 0.25 × 0.15	0.22 × 0.19 × 0.19	0.18 × 0.15 × 0.03	0.13 × 0.11 × 0.06	0.15 × 0.08 × 0.06
θ range for data collection	4.717 to 61.616	3.29 to 26.34	2.526 to 26.998	4.05 to 25.00	2.436 to 29.561
<i>h</i> , <i>k</i> , <i>l</i> ranges	−12 ≤ <i>h</i> ≤ 12, −24 ≤ <i>k</i> ≤ 24, −7 ≤ <i>l</i> ≤ 10	−11 ≤ <i>h</i> ≤ 9, −12 ≤ <i>k</i> ≤ 12, −13 ≤ <i>l</i> ≤ 13	−12 ≤ <i>h</i> ≤ 12, −13 ≤ <i>k</i> ≤ 13, −17 ≤ <i>l</i> ≤ 16	−8 ≤ <i>h</i> ≤ 11, −13 ≤ <i>k</i> ≤ 13, −17 ≤ <i>l</i> ≤ 16	−12 ≤ <i>h</i> ≤ 12, 0 ≤ <i>k</i> ≤ 15, −10 ≤ <i>l</i> ≤ 10
Completeness to θ (%)	97.4	99.10	97.0	83.3	99.9
Absorption correction	Semi-empirical from equivalents	Semi-empirical from equivalents	Semi-empirical from equivalents	Semi-empirical from equivalents	Semi-empirical from equivalents
Max. and min. transmission	1.00 and 0.0014	0.226 and 0.193	0.8511 and 0.4348	1.000 and 0.245	0.533 and 0.266
Refinement method	Full-matrix least-squares on <i>F</i> ²	Full-matrix least-squares on <i>F</i> ²	Full-matrix least-squares on <i>F</i> ²	Full-matrix least-squares on <i>F</i> ²	Full-matrix least-squares on <i>F</i> ²
Data/parameters	2951/263	3753/241	5348/389	4605/388	4086/191
Goodness-of-fit on <i>F</i> ²	0.999	1.145	1.025	1.003	1.050
Final <i>R</i> indices [<i>I</i> > 2 σ (<i>I</i>)]	<i>R</i> ₁ = 0.0721, <i>wR</i> ₂ = 0.1757	<i>R</i> ₁ = 0.0294, <i>wR</i> ₂ = 0.0670	<i>R</i> ₁ = 0.0388, <i>wR</i> ₂ = 0.0823	<i>R</i> ₁ = 0.0509, <i>wR</i> ₂ = 0.1336	<i>R</i> ₁ = 0.0217, <i>wR</i> ₂ = 0.0461
<i>R</i> indices (all data)	<i>R</i> ₁ = 0.0854, <i>wR</i> ₂ = 0.1875	<i>R</i> ₁ = 0.0330, <i>wR</i> ₂ = 0.0703	<i>R</i> ₁ = 0.0569, <i>wR</i> ₂ = 0.0900	<i>R</i> ₁ = 0.0577, <i>wR</i> ₂ = 0.1367	<i>R</i> ₁ = 0.0229, <i>wR</i> ₂ = 0.0467
Largest diff. peak and hole (e Å ⁻³)	2.953 and −3.287	2.503 and −1.387	1.158 and −0.803	1.679 and −1.768	0.586 and −0.862
CCDC number	1840504	1840505	1840506	1840507	1840508

Results and discussion

Description of the structures

The ellipsoid plots of the asymmetric unit for the title Pb compounds (1–5) are illustrated in Fig. 2, 4, 6, 8 and 10 with

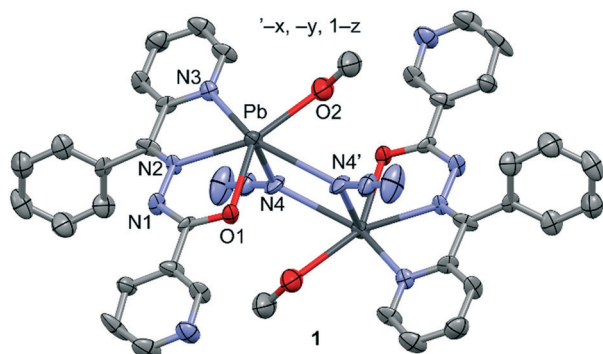


Fig. 2 Ortep view (H atoms are omitted for clarity) of 1. The thermal ellipsoids are drawn at a 50% probability level.

a partial atom numbering scheme. Selected bond lengths and bond angles around the metal centre of all the compounds are included in Table S1.† The bond lengths and angles in the organic ligands are normal for coordinated Schiff bases.³⁵ The X-ray crystallography reveals that the title compounds exhibit a variety of hydrogen bonds, C–H⋯ π , π – π stacking and lone-pair (l.p)⋯ π interactions (see Tables S2–S4†) in the solid state. The descriptions of these interactions are provided in detail in the ESI.† We are more interested to analyse the less studied tetrel bonding interactions in the title compounds (1–5) as detailed below.

In some cases, it is difficult to differentiate if the Pb⋯X (X = N, O, S, Br) interactions discussed herein are noncovalent tetrel bonding contacts or coordination bonds with a partial covalent character. Several coordination bonds observed in the structures, sometimes due to the rigidity of the ligand, are longer than the sum of covalent radii (ΣR_{cov}) and much shorter than the sum of van der Waals radii (ΣR_{vdw}). However, other coordination bonds (for instance solvent molecules) are much longer than the ΣR_{cov} . These

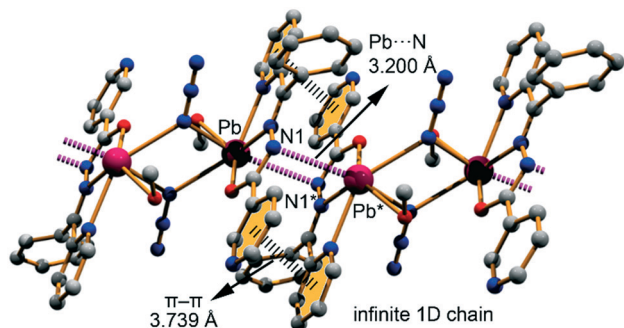


Fig. 3 Self-assembled dimeric unit generated through Pb...N tetrel bonds (pink dotted lines) in (1). The symmetry operation used to generate equivalent atoms is $* = -x, -y, -z$.

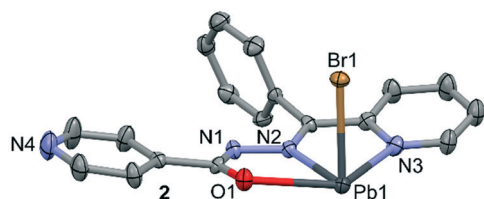


Fig. 4 Ortep view (H atoms are omitted for clarity) of 2. The thermal ellipsoids are drawn at a 50% probability level.

interactions can be thus considered as noncovalent tetrel bonding. Therefore, a criterion is needed to differentiate both bonds. Herein, we propose a simple criterion that consists of using half of the sum of covalent and van der Waals radii as the separation value to differentiate coordination bonds from tetrel bonding interactions. The values are gathered in Table 2.

Compound (1) crystallizes in the $P2_1/c$ space group of the monoclinic system and its structure consists of $\mu_{1,1}$ -azido bridged dinuclear units of Pb(II) where the metal ion exhibits a coordination number of 6. The dimer is based on a crystallographic inversion center ($-x, -y, 1 - z$) and the azido bridges connect the symmetry-related Pb ions in a basal-axial fashion (Fig. 2). It can be observed that the coordination of each Pb is totally hemidirectional with the ligands (L^1) occupying only half of the coordination sphere, that is, O1, O2, N2, N3 and N4' atoms at the basal plane and N4 at the apical position (pentagonal pyramid geometry).

Interestingly, the dinuclear units generate an infinite 1D chain in the solid state through Pb...N tetrel bonds (see Fig. 3). The Pb...N tetrel bonds are symmetrically equivalent with a separation distance of 3.200(2) Å, which is longer than half of the sum of covalent radii and van der Waals radii, $1/2(\Sigma R_{vdw} + \Sigma R_{cov}) = 2.87$ Å. The dimers are also stabilised by a pair of hydrogen bonds (of 2.785(3) Å) between the methanol molecule coordinated to one Pb centre and the oxygen atom of the L^1 ligand coordinated to the other. The assembly is further stabilized by the formation of electrostatically enhanced π - π interactions between the π -basic uncoordinated pyridine and the π -acidic Pb-coordinated pyridine ring, as described in the theoretical study (*vide infra*). It should be men-

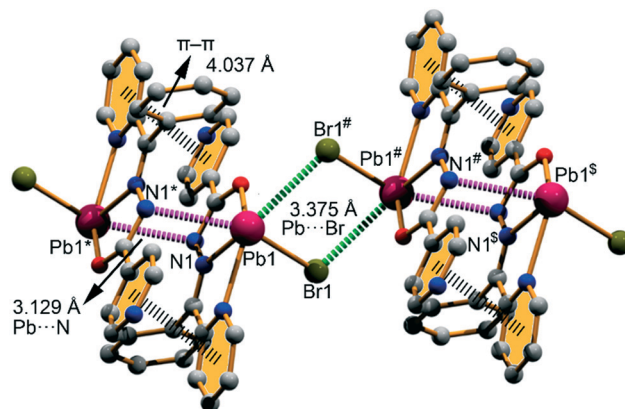


Fig. 5 Self-assembled network in (2) generated through Pb...N (pink dotted lines) and Pb...Br (green dotted lines) tetrel bonds. The symmetry operations used to generate the equivalent atoms are as follows: $* = -x, 2 - y, -z$; $\# = 1 - x, 2 - y, -z$; $\$ = 1 + x, y, z$.

tioned that the coordinated methanol molecule presents a coordination distance (2.91 Å) that is also significantly longer than $1/2(\Sigma R_{vdw} + \Sigma R_{cov}) = 2.78$ Å. Therefore, the Pb coordination number in complex 1 can be considered to be $n = 5$ and the solvent molecule forms a noncovalent Pb...O tetrel bond with the metal center.

Compound 2 crystallizes in the triclinic $P\bar{1}$ space group. The Pb ion is coordinated by one NNO donor organic ligand (L^2) and the fourth site is occupied by the Br ion (Fig. 4). The spatial distribution of the ligands is clearly hemidirectional with more than half of the coordination sphere of Pb available for establishing noncovalent interactions (see Fig. 4).

Apart from other weak noncovalent interactions described in the ESI,[†] the solid-state structure of 2 exhibits two types (Pb...N and Pb...Br) of tetrel bonding interactions. First, the parent molecule is in contact with the partner molecule at $(-x, 2 - y, -z)$ through symmetrically equivalent Pb...N tetrel bonds with a separation distance 3.129 Å. Thus, a centrosymmetric dimeric motif is generated through tetrel bonds in 2 (see Fig. 5).

The P...N distance (3.129 Å) is longer than $1/2(\Sigma R_{vdw} + \Sigma R_{cov}) = 2.87$ Å. Due to the self-complementary nature of the molecules, the dimeric units are again juxtaposed through Pb...Br tetrel bonding interactions and the combination of these two bonds leads the molecules to propagate along the [100] direction (Fig. 5), generating a supramolecular 1D polymeric chain. Similar to compound 1, electrostatically

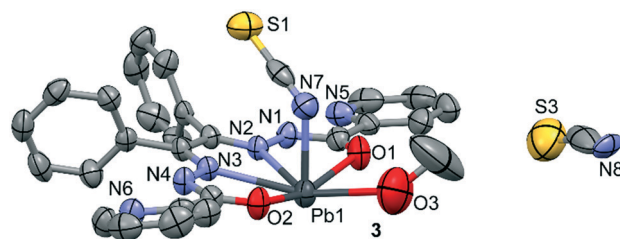


Fig. 6 Ortep view (H atoms are omitted for clarity) of 3. The thermal ellipsoids are drawn at a 50% probability level.

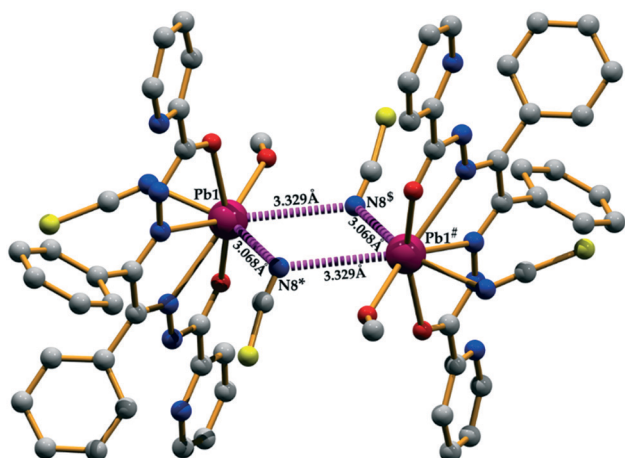


Fig. 7 Perspective view of the Pb...N (pink dotted lines) tetrel bonds in (3). The symmetry operations used to generate the equivalent atoms are as follows: * = $1 + x, y, z$; # = $2 - x, 2 - y, 1 - z$; \$ = $1 - x, 2 - y, 1 - z$.

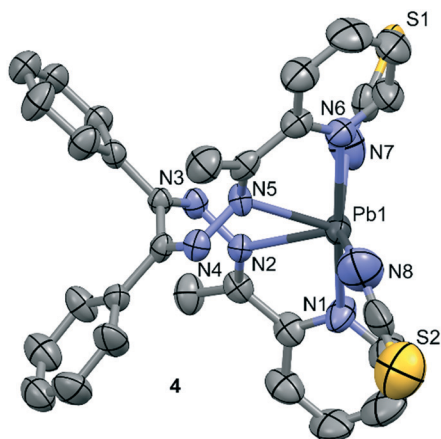


Fig. 8 Ortep view (H atoms are omitted for clarity) of 4. The thermal ellipsoids are drawn at a 50% probability level.

enhanced π - π interactions are also present in the assembly. In addition, the water molecule also participates in tetrel bonding interactions [the Pb...O2 distance is 2.932(4) Å], as highlighted in Fig. S2.†

Compound 3 crystallizes in the triclinic $P\bar{1}$ space group where the Pb metal center is coordinated to two nitrogen and two oxygen atoms of the N_2O_2 donor ligand (H_2L^3). One nitrogen atom and one oxygen atom from thiocyanate and methanol molecules, respectively, complete the PbN_3O_3 coordination sphere ($n = 6$) (see Fig. 6). Similar to the behaviour

Table 2 Covalent (R_{cov}) and van der Waals radii (R_{vdw}) of the Pb and donor atoms (X) that participate in tetrel bonding interactions

Atom	R_{cov}	R_{vdw}	ΣR_{cov} (Pb + X)	ΣR_{vdw} (Pb + X)	$1/2(\Sigma R_{vdw} + \Sigma R_{cov})$
Pb	1.46	2.02	—	—	—
X = N	0.71	1.55	2.17	3.57	2.87
X = O	0.66	1.52	2.02	3.54	2.78
X = S	1.05	1.80	2.51	3.82	3.17
X = Br	1.20	1.85	2.66	3.87	3.26

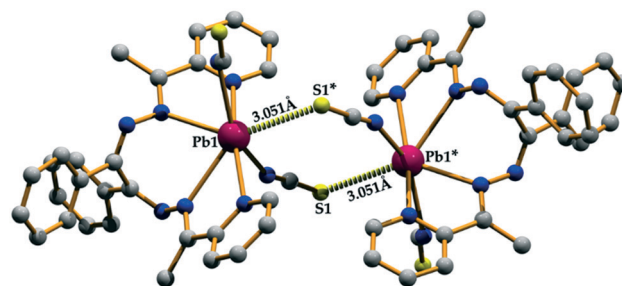


Fig. 9 Formation of a dimeric unit through Pb...S contacts (yellow dotted lines) in (4). The symmetry operation used to generate the equivalent atoms is * = $1 - x, 1 - y, 1 - z$.

previously described for 1, the coordination of Pb is hemidirectional with the ligands L^3 , MeOH and SCN^- occupying only half of the coordination sphere, exhibiting a pentagonal pyramid geometry.

Apart from the lone-pair (l.p) $\cdots \pi$ and π - π stacking interactions described in the ESI,† compound 3 generates a dimeric motif through a pair of Pb...N tetrel bonding contacts. Two nitrogen atoms from two symmetrically different thiocyanate molecules are in contact with the Pb atoms of parent and partner molecules to build the supramolecular assembly. The separation distances between the nitrogen atoms and the Pb atoms of the parent and partner molecules are 3.068(9) Å and 3.329(8) Å, respectively (Fig. 7). Both the Pb...N distances are significantly longer than $1/2(\Sigma R_{vdw} + \Sigma R_{cov}) = 2.87$ Å, confirming the noncovalent nature of the interaction, as further analysed below. Similarly to 1, the coordinated MeOH also participates in the assembly of the dimers as a hydrogen bond donor; however, unlike in 1, the bridging pseudohalide also acts as a hydrogen bond donor. The hydrogen bond is formed with the sulphur atom of the thiocyanate and is fairly long (O...S distance of 3.554(6) Å) indicating that the Pb...N tetrel bond is the dominant interaction within a dimer. This result is somewhat reminiscent of the previously noted dominance of halogen bonds (also a σ -hole interaction!) over hydrogen bonds in cocrystals of (N-halogeno)imides.³⁶

Compound 4 crystallizes in the triclinic $P\bar{1}$ space group where the Pb atom is coordinated to four nitrogen atoms of the ligand (L^4) and two additional coordination positions are

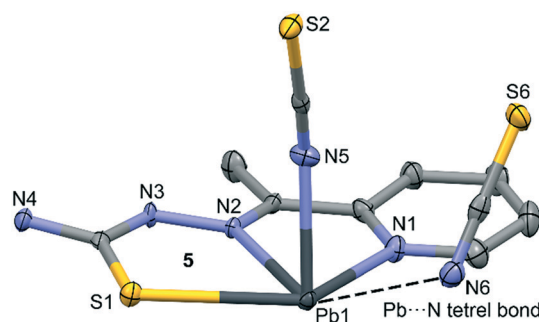


Fig. 10 Ortep view (H atoms are omitted for clarity) of 5. The thermal ellipsoids are drawn at a 50% probability level.

occupied by the nitrogen atoms of two thiocyanate molecules (Fig. 8). The coordination of Pb is basically hemidirectional with the ligands L^4 and SCN^- occupying only half of the coordination sphere, exhibiting a distorted trigonal prismatic geometry.

The Pb ion is in contact with the S atom of the partner molecule at $(1 - x, 1 - y, 1 - z)$ through $Pb \cdots S$ interactions, which leads to the formation of a centrosymmetric dimeric motif (Fig. 9). The contact is established between the S(1) atom of the N-coordinated pseudohalide ligand and the Pb(1) atom and is characterized by an interatomic distance of 3.051(2) Å, which is slightly shorter than $1/2(\Sigma R_{vdW} + \Sigma R_{cov}) = 3.17$ Å. In this particular case, the interaction could be considered to be close to the limit of a very long coordination bond. In any case, this self-complementary interaction plays a crucial role in the formation of a supramolecular dimer (Fig. 9) whereas another dimeric unit is generated through π -stacking interaction, as discussed in the ESI†

Compound 5 crystallizes in the monoclinic space group Pc where the Pb ion coordinates to three atoms of the Schiff base ligand and one nitrogen atom of the pseudohalide ligand occupies the fourth position (Fig. 10). Moreover, an outer-sphere thiocyanate counter-ion is present to counterbalance the cationic complex. Again $Pb(II)$ presents a hemidirectional coordination ($n = 4$), leaving a large void for establishing non-covalent tetrel bonding interactions.

In addition to the $Pb1 \cdots N6$ tetrel bonding interaction (see Fig. 10), three additional $Pb \cdots S$ tetrel bonds are established in the solid state (see Fig. 11 and S6†), thus confirming the ability of the $Pb(II)$ atom to participate in σ -hole interactions. In Fig. 11, we show the tetrel bonds that are formed between the S(1) atom of the ligand molecule and the S(2) atom of the N-coordinated pseudohalide ligand and the Pb atom of the partner molecule at $(x, -y, -1/2 + z)$. These two $Pb \cdots S$ tetrel bonds are characterized by an interatomic distance of 3.229(2) Å and 3.409(2) Å, respectively. The third $Pb \cdots S$ tetrel bond also involves the S2 of another molecule at $(x, y, z + 1)$ and the distance is 3.380(2) Å; see Fig. S6 (ESI†). These three separation distances are longer than $1/2(\Sigma R_{vdW} + \Sigma R_{cov}) = 3.17$ Å, thus suggesting the noncovalent nature of the interactions (Fig. 11).

Hirshfeld surfaces

The Hirshfeld surfaces of compounds 1–5 are mapped over d_{norm} and are depicted in Fig. S6† and in Fig. 12 only for compound 4 as an exemplifying model. The dominant intermolecular interactions are evidenced by the circular depressions on the d_{norm} surfaces (Fig. S7† and 12a and b). We are particularly interested to investigate if the $Pb \cdots N$, $Pb \cdots Br$ and $Pb \cdots S$ tetrel bonds can also be evidenced by means of Hirshfeld surface analysis. Gratifyingly, the tetrel bonds were characterized by the spikes of the breakdown fingerprint plots (Fig. S8† and 12c and d).

The proportions of $Pb \cdots N/N \cdots Pb$ interactions comprise 3.5%, 2.1%, 2.2%, 0.0% and 1.0% of the total Hirshfeld sur-

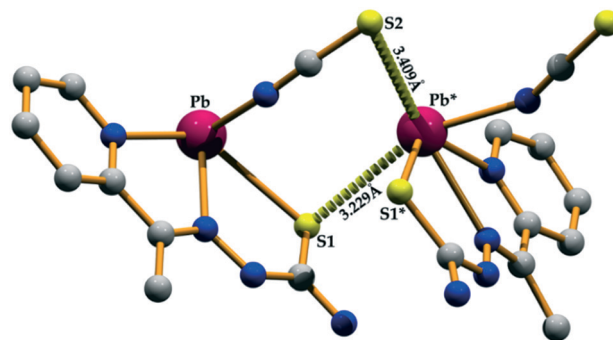


Fig. 11 Perspective view of the $Pb \cdots S$ tetrel bonds (yellow dotted lines) in (5). The symmetry operation used to generate the equivalent atoms is $* = x, -y, -1/2 + z$.

face area of 1–5, respectively. As described above, compound 4 does not exhibit a $Pb \cdots N/N \cdots Pb$ tetrel bond and it is evidenced (no scattered points/spikes are visible) by the breakdown fingerprint plot (Fig. S8†). Compound 2 exhibits $Pb \cdots Br/Br \cdots Pb$ tetrel bonds that contribute 1.7% of the total Hirshfeld surface area and are evident in the (d_i, d_e) region of (1.791 Å, 1.283 Å) (Fig. S7†). No significant $Pb \cdots S/S \cdots Pb$ interactions are observed in compound 3. However, the molecular interactions in compounds 4 and 5 in terms of $Pb \cdots S/S \cdots Pb$ contacts are reflected in the distribution of the scattered points on the fingerprint plots (see Fig. 12c and d and S7†). A close inspection of the fingerprint plots revealed that the sharp spikes with the shortest $(d_e + d_i) = 3.098$ Å in 4 and $(d_e + d_i) = 3.273$ Å in 5 correspond to $Pb \cdots S/S \cdots Pb$ interactions. It is worth noting that in the structure of 4, those contacts are much more dispersed and cover only 1.5% of the Hirshfeld surface compared to 6.3% in 5.

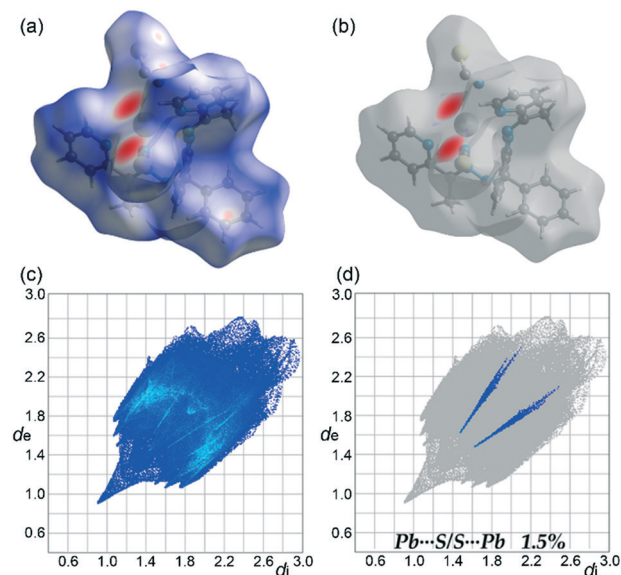


Fig. 12 (a) Hirshfeld surface mapped with d_{norm} for complex 4. (b) The $Pb \cdots S/S \cdots Pb$ contribution to the Hirshfeld surfaces is shown. (c) Full fingerprint plot of 4. (d) Fingerprint plot resolved into a $Pb \cdots S$ tetrel bond showing its contribution.

Theoretical study

We have focused the theoretical study on the comparison of the energetic features of the tetrel bonding interactions observed in the solid-state crystal structures of compounds 1–4 described above.

For compound 1, we have studied the self-assembled dimer mentioned above and highlighted in Fig. 3. First of all, we have computed the molecular electrostatic potential (MEP) surface of compound 1 (see Fig. 13a) plotted onto the van der Waals surface. The presence of a strong σ -hole (+17 kcal mol⁻¹) in the Pb atom at the extension of the N–Pb bond can be observed, represented in blue. The electrostatic potential at the N atom of pyridine is negative (–44.5 kcal mol⁻¹); however in the solid state it establishes H-bonding interactions with the aromatic H atoms of the coordinated pyridine (enhanced the acidity of the coordination). Interestingly, the uncoordinated N atom of the –N=N–C(O)– group of the ligand also presents a negative MEP value (–30 kcal mol⁻¹, see Fig. 13a) thus indicating that the tetrel bond is electrostatically very favourable. We

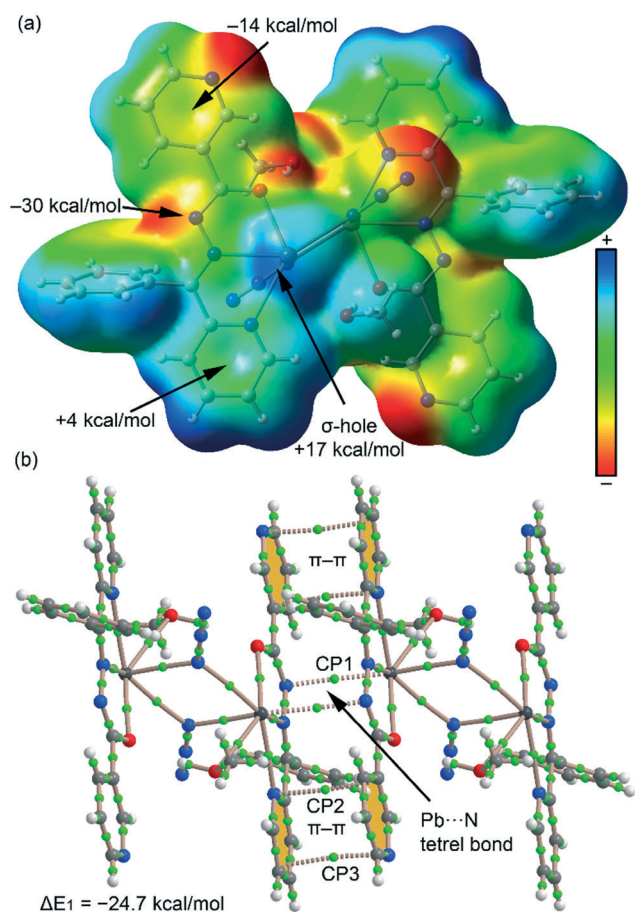


Fig. 13 (a) MEP surface of compound 1 plotted onto the van der Waals surface (isovalue 0.001 a.u.). The MEP values at selected points of the surface are given. (b) AIM distribution of bond critical points (green spheres) and bond paths. For clarity, only the CPs and bond paths that characterize the covalent and noncovalent intermolecular interactions are given.

have computed the interaction energy of the self-assembled dimer (see Fig. 13b), which is large and negative ($\Delta E_1 = -24.7$ kcal mol⁻¹) due to the formation of two symmetrically equivalent tetrel bonds. We have used Bader's theory of atoms in molecules to characterize the interactions. The existence of a bond critical point (CP) and a bond path connecting two atoms is a clear evidence of interaction,³⁷ since it indicates that the electron density is accumulated between the nuclei that are linked by the associated atomic interaction line.³³ In Fig. 13b, we represent the distribution of CPs and bond paths of the dimer and it shows that each tetrel bond is characterized by a bond CP (green sphere) and a bond path connecting the Pb atom to the N atoms ($\rho_{\text{BCP1}} = 0.0132$ a.u.). Moreover, the distribution of bond CPs also reveals the existence of π – π stacking interactions between the pyridine rings that are characterized by two bond CPs and a bond path interconnecting the N and C atoms ($\rho_{\text{BCP2}} = 0.0065$ a.u. and $\rho_{\text{BCP3}} = 0.0051$ a.u.). This π – π stacking interaction is electrostatically enhanced, since the MEP value over the center of the coordinated pyridine ring is positive (+4 kcal mol⁻¹, Fig. 13a) due to its coordination to the metal center and the MEP value over the center of the other pyridine ring is negative (–14 kcal mol⁻¹, Fig. 13a). In an effort to evaluate the contribution of this π – π stacking interaction, we have computed the dimerization energy of a theoretical model where the uncoordinated pyridine has been replaced by a H atom. Consequently, the π – π stacking interaction is not established and the binding energy is reduced to $\Delta E_1(\text{Py} \rightarrow \text{H}) = -16.9$ kcal mol⁻¹ which corresponds to both tetrel bonding interactions and the difference (–7.8 kcal mol⁻¹) is the contribution of the π – π stacking interactions.

The combination of interactions (Pb...N tetrel and π -stacking interactions) described in the assembly analysed above for 1 is also observed in compound 2 (highlighted in Fig. 5 using pink dotted lines). Thus, in compound 2 we have only focused the theoretical study on the analysis of the Pb...Br tetrel bonding interactions (also highlighted in Fig. 5 using green dotted lines). In Fig. 14, we show the MEP surface of compound 2 and the distribution at the Pb atom is anisotropic with two regions (σ -holes) with MEP values of +32 and +35 kcal mol⁻¹, thus suitable for establishing strong tetrel bonds. The MEP surface also indicates that the most negative region corresponds to the N atom of the uncoordinated pyridine ring (–43 kcal mol⁻¹). However, in the solid state this position is blocked by the presence of an H-bonded water molecule (see Fig. 4). The bromide ligand also presents a large and negative MEP value (–37 kcal mol⁻¹) thus adequate for the interaction with the Pb atom. The interaction energy of the self-assembled dimer is, consequently, very favourable ($\Delta E_2 = -17.3$ kcal mol⁻¹). The AIM analysis shown in Fig. 14b confirms the existence of both Pb...Br tetrel bonds that are characterized by a bond CP and a bond path interconnecting the Pb and Br atoms ($\rho_{\text{BCP4}} = 0.0153$ a.u.). The interaction is further characterized by the presence of a ring CP (yellow sphere) due to the formation of a supramolecular ring.

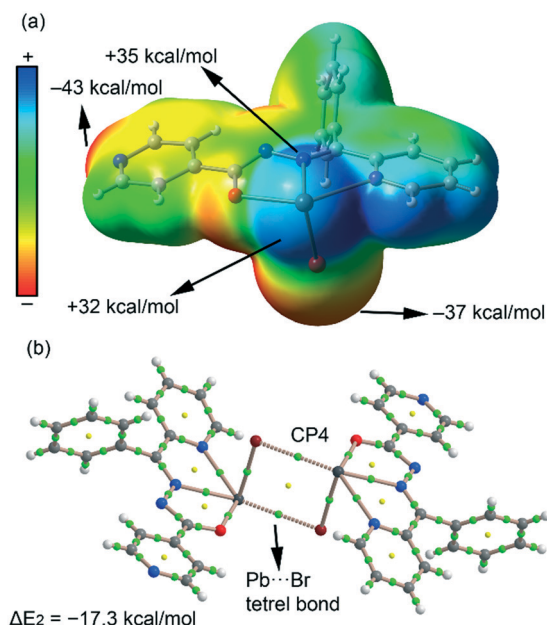


Fig. 14 (a) MEP surface of compound 2 plotted onto the van der Waals surface (isovalue 0.001 a.u.). The MEP values at selected points of the surface are given. (b) AIM distribution of bond and ring critical points (green and yellow spheres, respectively) and bond paths of the self-assembled dimer of compound 2.

In compound 3, the organic ligand is neutral and one of the pseudohalide counterions (SCN^-) is not covalently bonded to the Pb(II) metal center. In fact, Pb(II) establishes

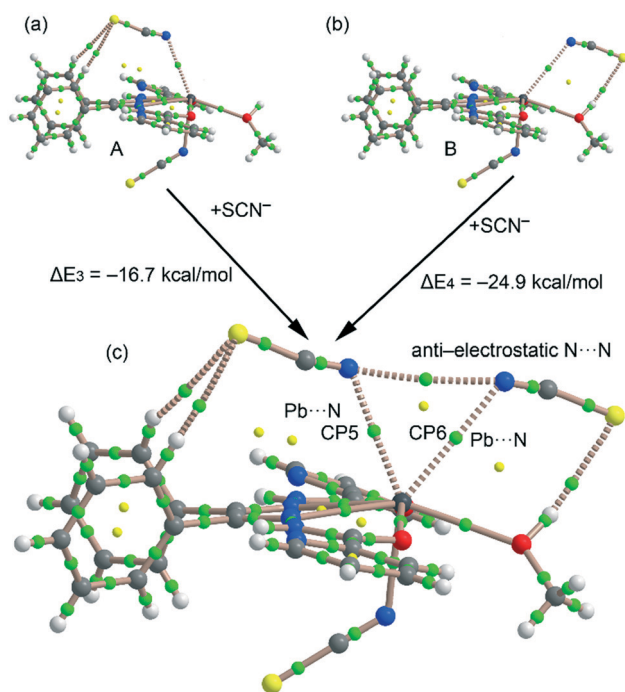


Fig. 15 (a) AIM distribution of the neutral assembly A. (b) AIM distribution of the neutral assembly B. (c) and (b) AIM distribution of bond and ring critical points (green and yellow spheres, respectively) and bond paths of the ternary assembly in compound 3.

two tetrel bonding interactions with two out-of-sphere ligands, as highlighted in Fig. 7. In order to estimate the tetrel bonding interactions using a neutral model (to minimize pure electrostatic ion pair interactions), we have computed the interaction energy using two different possibilities, as represented in Fig. 15. First, we considered that the neutral assembly 'A' was previously formed (see Fig. 15a) and evaluated the formation of the ternary system. The binding energy is $\Delta E_3 = -16.7 \text{ kcal mol}^{-1}$ and it accounts for the tetrel bonding interaction and two weak $\text{C-H}\cdots\text{S}$ H-bonds, as revealed by the AIM distribution of CPs (see Fig. 15c). Secondly, we considered that the neutral assembly 'B' was already formed (see Fig. 15b) and we evaluated the interaction with the anion. In this case, the interaction energy is larger, $\Delta E_4 = -24.9 \text{ kcal mol}^{-1}$, because a strong H-bonding interaction is also formed between the coordinated MeOH and the S atom of the pseudohalide. The distribution of CPs (see Fig. 15c) of the ternary assembly shows that each tetrel bonding interaction is characterized by a bond CP and a bond path ($\rho_{\text{BCP5}} = 0.0145 \text{ a.u.}$ and $\rho_{\text{BCP6}} = 0.0090 \text{ a.u.}$) connecting the Pb to the N atom. Moreover, the AIM analysis also shows a bond CP and a bond path connecting both pseudohalides, which is an unambiguous indication of the existence of a $\text{N}\cdots\text{N}$ interaction. It should be emphasized that the presence of a bond CP

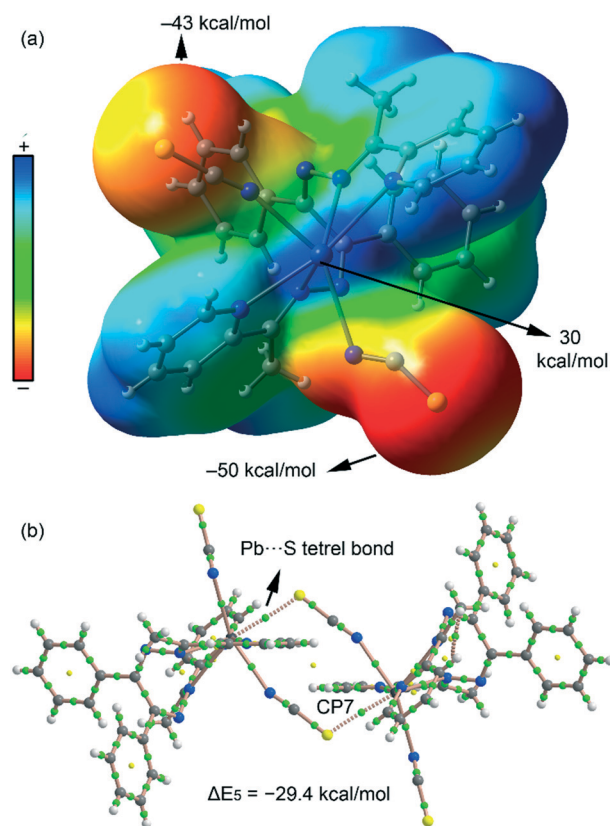


Fig. 16 (a) MEP surface of compound 4 plotted onto the van der Waals surface (isovalue 0.001 a.u.). The MEP values at selected points of the surface are given. (b) AIM distribution of bond and ring critical points (green and yellow spheres, respectively) and bond paths of the self-assembled dimer of compound 4.

does not imply that the interaction is attractive. In fact, this contact can be considered as an example of anti-electrostatic anion–anion interaction.

Finally, in compound 4 we have analysed the formation of the self-assembled dimer *via* the Pb···S interactions (highlighted in Fig. 9). In Fig. 16a we show the MEP surface of compound 4 and it shows an accessible σ -hole at the Pb atom (+30 kcal mol^{−1}), thus suitable for establishing strong interactions with electron-rich atoms. The MEP surface also indicates that the most negative region corresponds to the S atom of the pseudohalide (−50 kcal mol^{−1}), thus adequate for the interaction with the Pb atom. The interaction energy of the self-assembled dimer is, consequently, very favorable (ΔE_5 = −29.4 kcal mol^{−1}) since two long Pb···S coordination bonds are established. The AIM analysis shown in Fig. 16b confirms the existence of both Pb···S interactions that are characterized by a bond CP and a bond path interconnecting the Pb and S atoms ($\rho_{\text{BCP7}} = 0.0260$ a.u.).

Conclusions

In conclusion, we report the syntheses and structural characterization of five new Pb²⁺ complexes with several organic ligands and anionic co-ligands. In all the compounds (1–5), the Pb(II) ion exhibits a hemidirectional coordination, even in those with a coordination index of $n = 6$. All the compounds present relevant Pb···X (X = O, N, S, Br) tetrel bonding interactions in the solid state which have been described and evaluated using DFT calculations. We have proposed a simple criterion to differentiate coordination bonds from noncovalent tetrel bonds. The binding energies have been calculated and they range from moderate to strong depending on the Pb²⁺ environment. The electrostatic contribution, as shown by the MEP surface plots, is very important to describe the tetrel bonding. Our results are expected to be important to understanding the X-ray structure of supramolecular MOFs that contain hemidirectionally coordinated lead(II) centres and anionic or neutral organic ligands.

Conflicts of interest

There are no conflicts to declare.

Acknowledgements

S. K. Seth is grateful to the SERB-DST (Govt. of India) for the Overseas Postdoctoral Fellowship (SB/OS/PDF-524/2015-16). G. M. is grateful to the University of Maragheh for the financial support of this research (Agreement number 95.1726). A. B. and A. F. thank the MINECO/AEI of Spain (projects CTQ2014-57393-C2-1-P and CTQ2017-85821-R). A. B. and A. F. thank the CTI (UIB) for computational facilities.

Notes and references

- (a) R. M. Harrison and D. R. H. Laxen, *Lead Pollution*, Chapman & Hall, London, 1981; (b) B. P. Lanphear, D. A. Burgoon, S. W. Rust, S. Eberly and W. Galke, *Environ. Res.*, 1998, **76**, 120–130; (c) T. G. Spiro and W. M. Stigliani, *Chemistry of the Environment*, Prentice Hall, Upper Saddle River, NJ, 1996; (d) F. Cuenot, M. Meyer, A. Bucaille and R. Guillard, *J. Mol. Liq.*, 2005, **118**, 89–99; (e) R. A. Goyer, in *Handbook on Toxicity of Inorganic Compounds*, ed. H. G. Seiler, H. Sigel and A. Sigel, Marcel Dekker, New York, 1988.
- (a) A. Morsali and A. R. Mahjoub, *Helv. Chim. Acta*, 2004, **87**, 2717–2722; (b) H. Fleischer and D. Schollmeyer, *Inorg. Chem.*, 2004, **43**, 5529–5536; (c) D. L. Reger, T. D. Wright, C. A. Little, J. J. S. Lamba and M. D. Smith, *Inorg. Chem.*, 2001, **40**, 3810–3814; (d) R. D. Hancock, J. H. Reibenspies and H. Maumela, *Inorg. Chem.*, 2004, **43**, 2981–2987; (e) C. Platas-Iglesias, D. Esteban-Gomez, T. Enriquez-Perez, F. Avecilla, A. de Blas and T. Rodríguez-Blas, *Inorg. Chem.*, 2005, **44**, 2224–2233.
- (a) F. Cheng, J. Liang, Z. Tao and J. Chen, *Adv. Mater.*, 2011, **23**, 1695–1715; (b) L. Zhang, Y.-Y. Qin, Z.-J. Li, Q.-P. Lin, J.-K. Cheng, J. Zhang and Y.-G. Yao, *Inorg. Chem.*, 2008, **47**, 8286–8293; (c) A. Olvera, G. Shi, H. Djieutedjeu, A. Page, C. Uher, E. Kioupakis and P. F. P. Poudeu, *Inorg. Chem.*, 2015, **54**, 746–755.
- (a) C. L. Seaton, J. Lasman and D. R. Smith, *Toxicol. Appl. Pharmacol.*, 1999, **159**, 153–160; (b) D. E. Glotzer, K. A. Freedberg and H. Baucher, *Med. Decis. Making*, 1995, **15**, 13–24; (c) D. E. Glotzer and H. Baucher, *Pediatrics*, 1992, **89**, 614–618; (d) M. E. Markowitz and J. F. Rosen, *J. Pediatr.*, 1991, **119**, 305–310.
- (a) S.-R. Fan and L.-G. Zhu, *Inorg. Chem.*, 2007, **46**, 6785–6793; (b) R. Ferreirs-Martinez, D. Esteban-Gomez, E. Toth, A. de Blas, C. Platas-Iglesias and T. Rodríguez-Blas, *Inorg. Chem.*, 2011, **50**, 3772–3784; (c) J. M. Ratcliffe, *Lead in Man and Environment*, John Wiley & Sons, New York, 1981; (d) M. D. J. J. Chisolm Jr, *J. Pediatr.*, 1968, **73**, 1–38.
- (a) T.-T. Liu, J. Liang, Y.-B. Huang and R. Cao, *Chem. Commun.*, 2016, **52**, 13288–13291; (b) Y. Huang, T. Liu, J. Lin, J. Lü, Z. Lin and R. Cao, *Inorg. Chem.*, 2011, **50**, 2191–2198; (c) E. C. Constable, G. Zhang, C. E. Housecroft, M. Neuburger and J. A. Zampese, *CrystEngComm*, 2010, **12**, 1764–1773; (d) T. Nakajima, I. Shimizu, K. Kobayashi and Y. Wakatsuki, *Organometallics*, 1998, **17**, 262–269; (e) A. J. Tasiopoulos, T. A. O'Brien, K. A. Abboud and G. Christou, *Angew. Chem., Int. Ed.*, 2004, **43**, 345–349; (f) A. W. Coleman, D. F. Jones, P. H. Dixneuf, C. Brisson, J.-J. Bonnet and G. Lavigne, *Inorg. Chem.*, 1984, **23**, 952–956.
- (a) C. T. Lyons, T. Daniel and P. Stack, *Coord. Chem. Rev.*, 2013, **257**, 528–540; (b) P. G. Cozzi, *Chem. Soc. Rev.*, 2004, **33**, 410–421; (c) C. Baleizao and H. Garcia, *Chem. Rev.*, 2006, **106**, 3987–4043; (d) E. C. Constable, G. Zhang, C. E. Housecroft and J. A. Zampese, *Dalton Trans.*, 2010, **39**, 1941–1947.
- (a) X. Yang, B. P. Hahn, R. A. Jones, K. J. Stevenson, J. Steven Swinna and Q. Wu, *Chem. Commun.*, 2006, 3827–3829; (b) A. C. Sudik, A. R. Millward, N. W. Ockwig, A. P. Côté, J. Kim and O. M. Yaghi, *J. Am. Chem. Soc.*, 2005, **127**, 7110–7118; (c) A. V. Davis and K. N. Raymond, *J. Am. Chem. Soc.*, 2005, **127**, 7912–7919.

- 9 B. Dede, F. Kripcin and M. Cengiz, *J. Hazard. Mater.*, 2009, **163**, 1148–1156.
- 10 (a) F. He, M.-L. Tong and X.-M. Chen, *Inorg. Chem.*, 2005, **44**, 8285–8292; (b) Y. Sadaoka, E. Traversa and M. Sakamoto, *J. Mater. Chem.*, 1996, **6**, 1355–1360; (c) M. C. Carotta, G. Martinelli, Y. Sadaoka, P. Nunziante and E. Traversa, *Sens. Actuators, B*, 1998, **48**, 270–276.
- 11 (a) A. Jana, B. J. Crowston, J. R. Shewring, L. K. McKenzie, H. E. Bryant, S. W. Botchway, A. D. Ward, A. J. Amoroso, E. Baggaley and M. D. Ward, *Inorg. Chem.*, 2016, **55**, 5623–5633; (b) S. Realista, P. Ramgi, B. de P. Cardoso, A. I. Melato, A. S. Viana, M. J. Calhorda and P. N. Martinho, *Dalton Trans.*, 2016, **45**, 14725–14733; (c) M. I. Szavuly, M. Surducun, E. Nagy, M. Suranyi, G. Speier, R. Silaghi-Dumitrescu and J. Kaizer, *Dalton Trans.*, 2016, **45**, 14709–14718.
- 12 (a) N. V. Sidgwick and H. M. Powell, *Proc. R. Soc. London, Ser. A*, 1940, **176**, 153; (b) D. R. McKeney, *J. Chem. Educ.*, 1983, **60**, 112–116; (c) M. S. Banna, *J. Chem. Educ.*, 1985, **62**, 197–198; (d) K. S. Pitzer, *Acc. Chem. Res.*, 1979, **12**, 271–276; (e) P. Pyykkö and J.-P. Desclaux, *Acc. Chem. Res.*, 1979, **12**, 276–281; (f) P. Pyykkö, *Chem. Rev.*, 1988, **88**, 563–594.
- 13 (a) R. D. Hancock, J. H. Reibenspies and H. Maumela, *Inorg. Chem.*, 2004, **43**, 2981–2987; (b) R. Luckay, I. Cukrowski, J. Mashishi, J. H. Reibenspies, A. H. Bond, R. D. Rogers and R. D. Hancock, *J. Chem. Soc., Dalton Trans.*, 1997, 901–908; (c) A. Walsh and G. W. Watson, *J. Solid State Chem.*, 2005, **178**, 1422–1428; (d) R. D. Hancock, M. S. Shaikjee, S. M. Dobson and J. C. Boeyens, *Inorg. Chim. Acta*, 1988, **154**, 229–238; (e) D. Esteban-Gómez, C. Platas-Iglesias, T. Enriquez-Pérez, F. Avecilla, A. Blas and T. Rodríguez-Blas, *Inorg. Chem.*, 2006, **45**, 5407–5416; (f) C. Platas-Iglesias, D. Esteban-Gomez, T. Enriquez-Perez, F. Avecilla, A. D. Blas and T. Rodríguez-Blas, *Inorg. Chem.*, 2005, **44**, 2224–2233; (g) K. T. Mahmudov, M. N. Kopylovich, M. F. C. Guedes da Silva and A. J. L. Pombeiro, *Coord. Chem. Rev.*, 2017, **345**, 54–72; (h) K. T. Mahmudov, M. N. Kopylovich, M. F. C. Guedes da Silva and A. J. L. Pombeiro, *Dalton Trans.*, 2017, **46**, 10121–10138.
- 14 (a) P. Politzer, J. S. Murray and T. Clark, *Phys. Chem. Chem. Phys.*, 2013, **15**, 11178–11189; (b) A. Bauzá, T. J. Mooibroek and A. Frontera, *ChemPhysChem*, 2015, **16**, 2496–2517; (c) A. Bauzá and A. Frontera, *Angew. Chem., Int. Ed.*, 2015, **54**, 7340–7343.
- 15 (a) J. S. Murray, K. E. Riley, P. Politzer and T. Clark, *Aust. J. Chem.*, 2010, **63**, 1598–1607; (b) P. Politzer and J. S. Murray, *ChemPhysChem*, 2013, **14**, 278–294; (c) P. Politzer, J. S. Murray and T. Clark, *Phys. Chem. Chem. Phys.*, 2010, **12**, 7748–7757; (d) P. Politzer, K. E. Riley, F. A. Bulat and J. S. Murray, *Comput. Theor. Chem.*, 2012, **998**, 2–8; (e) A. Bauzá, I. Alkorta, A. Frontera and J. Elguero, *J. Chem. Theory Comput.*, 2013, **9**, 5201–5210; (f) G. Sánchez-Sanz, C. Trujillo, I. Alkorta and J. Elguero, *Phys. Chem. Chem. Phys.*, 2014, **16**, 15900–15909.
- 16 (a) A. Bauzá, T. J. Mooibroek and A. Frontera, *Angew. Chem., Int. Ed.*, 2013, **52**, 12317–12321; (b) S. J. Grabowski, *Phys. Chem. Chem. Phys.*, 2014, **16**, 1824–1834; (c) A. Bauzá, T. J. Mooibroek and A. Frontera, *Chem. – Eur. J.*, 2014, **20**, 10245–10248; (d) E. C. Escudero-Adán, A. Bauzá, A. Frontera and P. Ballester, *ChemPhysChem*, 2015, **16**, 2530–2533; (e) A. Bauzá, T. J. Mooibroek and A. Frontera, *Phys. Chem. Chem. Phys.*, 2014, **16**, 19192–19197; (f) A. Bauzá, T. J. Mooibroek and A. Frontera, *Chem. Commun.*, 2014, **50**, 12626–12629; (g) A. Bauzá, T. J. Mooibroek and A. Frontera, *Chem. Rec.*, 2016, **16**, 473–487; (h) J. S. Murray, P. Lane and P. Politzer, *J. Mol. Model.*, 2009, **15**, 723–729; (i) A. Bundhun, P. Ramasami, J. S. Murray and P. Politzer, *J. Mol. Model.*, 2013, **19**, 2739–2746; (j) R. S. Ruoff, T. Emilsson, A. I. Jaman, T. C. Germann and H. S. Gutowsky, *J. Chem. Phys.*, 1992, **96**, 3441–3446; (k) R.-D. Urban, G. Rouillé and M. Takami, *J. Mol. Struct.*, 1997, **413–414**, 511–519; (l) I. Alkorta, I. Rozas and J. Elguero, *J. Phys. Chem. A*, 2001, **105**, 743–749; (m) M. Servati Gargari, V. Stilinovic, A. Bauzá, A. Frontera, P. McArdle, D. Van Derveer, S. W. Ng and G. Mahmoudi, *Chem. – Eur. J.*, 2015, **21**, 17951–17958.
- 17 (a) G. Mahmoudi, S. K. Seth, A. Bauzá, F. I. Zubkov, A. V. Gurbanov, J. White, V. Stilinovic, T. Doert and A. Frontera, *CrystEngComm*, 2018, **20**, 2812–2821; (b) S. Roy, M. G. B. Drew, A. Bauzá, A. Frontera and S. Chattopadhyay, *New J. Chem.*, 2018, **42**, 6062; (c) G. Mahmoudi, A. Bauzá and A. Frontera, *Dalton Trans.*, 2016, **45**, 4965–4969.
- 18 C. Gourlaouen, O. Parisela and H. Gérard, *Dalton Trans.*, 2011, **40**, 11282–11288.
- 19 (a) C. Gourlaouen, O. Parisel and H. Gerard, *Dalton Trans.*, 2011, **40**, 11282–11288; (b) L. Shimoni-Livny, J. P. Glusker and C. W. Bock, *Inorg. Chem.*, 1998, **37**, 1853–1867; (c) R. L. Davidovich, V. Stavila, D. V. Marinin, E. I. Voit and K. H. Whitmire, *Coord. Chem. Rev.*, 2009, **253**, 1316–1352.
- 20 A. A. Khandar, B. K. Ghosh, C. Lampropoulos, M. S. Gargari, V. T. Yilmaz, K. Bhar, S. A. Hosseini-Yazdi, J. M. Cain and G. Mahmoudi, *Polyhedron*, 2015, **85**, 467–475.
- 21 Oxford Diffraction, *CrysAlis CCD and CrysAlis RED including ABSPACK, Version 171.32.29*, Oxford Diffraction Ltd, Wroclaw, Poland, 2003.
- 22 Agilent, *CrysAlis PRO*, Agilent Technologies Ltd, Yarnton, Oxfordshire, England, 2014.
- 23 Rigaku, *CrystalClear*, Rigaku Corporation, Tokyo, Japan, 2002.
- 24 Bruker, *SAINT*, Bruker AXS Inc., Madison, Wisconsin, USA, 2007.
- 25 Bruker, *SADABS*, Bruker AXS Inc., Madison, Wisconsin, USA, 2001.
- 26 G. M. Sheldrick, *Acta Crystallogr., Sect. A: Found. Crystallogr.*, 2008, **64**, 112–122.
- 27 (a) M. A. Spackman and J. J. McKinnon, *CrystEngComm*, 2002, **4**, 378–392; (b) J. J. McKinnon, M. A. Spackman and A. S. Mitchell, *Acta Crystallogr., Sect. B: Struct. Sci.*, 2004, **60**, 627–668.
- 28 (a) S. K. Seth, I. Saha, C. Estarellas, A. Frontera, T. Kar and S. Mukhopadhyay, *Cryst. Growth Des.*, 2011, **11**, 3250–3265; (b) P. Manna, S. K. Seth, A. Das, J. Hemming, R. Prendergast, M. Helliwell, S. R. Choudhury, A.

- Frontera and S. Mukhopadhyay, *Inorg. Chem.*, 2012, **51**, 3557–3571; (c) S. K. Seth, *CrystEngComm*, 2013, **15**, 1772–1781; (d) S. K. Seth, *J. Mol. Struct.*, 2014, **1064**, 70–75; (e) S. K. Seth, *J. Mol. Struct.*, 2014, **1070**, 65–74; (f) S. K. Seth, A. Bauzá and A. Frontera, *CrystEngComm*, 2018, **20**, 746–754; (g) T. Maity, H. Mandal, A. Bauza, B. C. Samanta, A. Frontera and S. K. Seth, *New J. Chem.*, 2018, **42**, 10202–10213.
- 29 (a) A. L. Rohl, M. Moret, W. Kaminsky, K. Claborn, J. J. Mckinnon and B. Kahr, *Cryst. Growth Des.*, 2008, **8**, 4517–4525; (b) A. Parkin, G. Barr, W. Dong, C. J. Gilmore, D. Jayatilaka, J. J. Mckinnon, M. A. Spackman and C. C. Wilson, *CrystEngComm*, 2007, **9**, 648–652; (c) S. K. Seth, D. Sarkar, A. D. Jana and T. Kar, *Cryst. Growth Des.*, 2011, **11**, 4837–4849; (d) S. K. Seth, D. Sarkar and T. Kar, *CrystEngComm*, 2011, **13**, 4528–4535; (e) T. Samanta, L. Dey, J. Dinda, S. K. Chattopadhyay and S. K. Seth, *J. Mol. Struct.*, 2014, **1068**, 58–70; (f) S. K. Seth, *Acta Crystallogr., Sect. E: Crystallogr. Commun.*, 2018, **74**, 600–606.
- 30 S. K. Wolff, D. J. Grimwood, J. J. McKinnon, D. Jayatilaka and M. A. Spackman, CrystalExplorer 3.1, The University of Western Australia, Perth, Australia, 2012.
- 31 R. Ahlrichs, M. Bär, M. Häser, H. Horn and C. Kölmel, *Chem. Phys. Lett.*, 1989, **162**, 165–169.
- 32 S. F. Boys and F. Bernardi, *Mol. Phys.*, 1970, **19**, 553–566.
- 33 R. F. W. Bader, *Chem. Rev.*, 1991, **91**, 893–928.
- 34 T. A. Keith, *AIMall (Version 13.05.06)*, TK Gristmill Software, Overland Park KS, USA, 2013.
- 35 A. Blagus, D. Cinčić, T. Friščić, B. Kaitner and V. Stilinović, *Maced. J. Chem. Chem. Eng.*, 2010, **29**, 117–138.
- 36 V. Stilinović, G. Horvat, T. Hrenar, V. Nemec and D. Cinčić, *Chem. – Eur. J.*, 2017, **23**, 5244–5257.
- 37 R. F. W. Bader, *J. Phys. Chem. A*, 1998, **102**, 7314–7323.